



This is a postprint version of the following published document:

Peña-Bahamonde, J., Atencia, J. J., Pozuelo, J., Tarazona, M. P. y Mendicuti, F. (2013): New Insights on the Self-Organization of PEG/ $\alpha$ -Cyclodextrin-Based Polyrotaxanes in Solution: An Experimental and Theoretical Study. *Macromolecular Chemistry and Physics*, 214 (24), pp.: 2801-2812.

DOI: [10.1002/macp.201300370](https://doi.org/10.1002/macp.201300370)

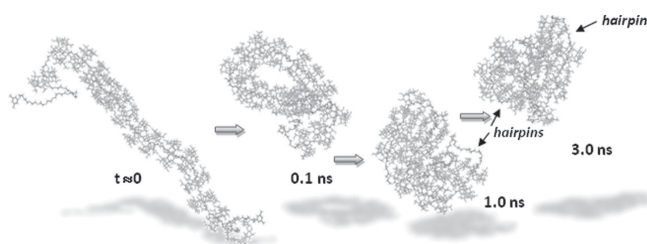
© WILEY, 2013

# New Insights on the Self-Organization of PEG/ $\alpha$ -Cyclodextrin-Based Polyrotaxanes in Solution: An Experimental and Theoretical Study

Janire Peña-Bahamonde, José Joaquín Atencia, Javier Pozuelo, María Pilar Tarazona, Francisco Mendicuti\*

Size exclusion chromatography coupled with light scattering (SEC/MALS), dynamic light scattering (DLS), steady-state and time-resolved fluorescence, as well as molecular dynamics (MD) simulations are used to study the behavior of several poly(ethylene glycol) (PEG)/  $\alpha$ -cyclodextrins ( $\alpha$  CDs) polyrotaxanes (PRs) in solution. The number of CD units in any of the PRs studied is always smaller than that required to saturate the PEG chains. These PRs seem to aggregate in dimethyl sulfoxide (DMSO) solution. The presence of hairpins in the non-saturated PRs contributes to diminishing their expected large dimensions. Intra- and inter-molecular interactions and forces responsible for hairpins and aggregation are investigated.

Keywords: fluorescence ; molecular dynamics ; poly(ethylene glycol) (PEG) ; polyrotaxane ; size exclusion chromatography



## 1. Introduction

In recent years, supramolecular polymers have attracted much research interest.<sup>[1-4]</sup> A classic example of these supramolecular structures is polyrotaxanes (PRs), which are formed by the nonbonded interactions of hollow macrocycles threaded onto a single linear polymer chain.<sup>[4-9]</sup> Cyclodextrins (CDs) are a more-common macrocycle.<sup>[10-16]</sup> Among them, the most used are the native  $\alpha$ -,  $\beta$ -, and  $\gamma$ CDs composed of 6, 7, and 8 D(+)-glucopyranose units connected by  $\alpha$ -1,4-linkages, respectively. Their relatively hydrophobic cavities make the inclusion of a variety of guest molecules including polymers possible. The major

driving forces for forming PRs are usually hydrophobic and van der Waals interactions between the CD and the polymer chain.<sup>[9]</sup> The first PRs formed by spontaneous inclusion of linear polymers with CDs were reported more than 20 years ago and poly(ethylene glycol) (PEG)/ $\alpha$ CDs were the first obtained in a crystalline state.<sup>[17,18]</sup> The formation of these PRs depended not only on the nature and the molecular weight of the polymer but also on the cavity size.<sup>[19-22]</sup> Thus, PEG only formed spontaneously inclusion complexes with  $\alpha$ CDs and  $\gamma$ CDs in water but not with  $\beta$ CDs, which require more extreme conditions.<sup>[23]</sup> To prevent unthreading in solution, terminal bulky groups were added at both ends.<sup>[9-16,19-22,24,25]</sup> Differential thermal analysis (DTA) showed that the decomposition of these PRs occurred at higher temperatures than that of the free CDs, demonstrating the thermal stability of CDs in PRs.<sup>[26]</sup> Approximately 2.3 oxyethylene units per  $\alpha$ CD were found when the chain was completely saturated. Head-to-head (HH) orientation of CDs seemed to be more favorable than head-to-tail (HT) one.<sup>[24,27]</sup>

A wide variety of materials have been prepared from the PRs derived from PEG or other linear polymers and CDs, such as molecular tubes,<sup>[28,29]</sup> drug carriers and

J. Peña-Bahamonde, Prof. M. P. Tarazona, Prof. F. Mendicuti Dpto. de Química Analítica, Química Física e Ingeniería Química, Universidad de Alcalá, 28871, Alcalá de Henares, Spain E-mail: francisco.mendicuti@uah.es

J. J. Atencia, Prof. J. Pozuelo

Dpto. de Ciencia e Ingeniería de Materiales e Ingeniería Química (IAAB), Universidad Carlos III de Madrid Leganés, Spain

delivery systems,<sup>[30]</sup> multivalent ligands that possess rotating/sliding recognition groups,<sup>[31]</sup> molecular wires using a CD molecular tube as insulator for conducting polymers,<sup>[32–36]</sup> PR/cellulose blend fibers showing good elongation properties,<sup>[37]</sup> and cross-linked PR materials with diverse mechanical responses.<sup>[38–44]</sup>

One of the major problems with the characterization in solution of the PEG/CD-based PRs, particularly with high CD coverage, is that they are hardly soluble in water and most regular organic solvents, like dimethylformamide or pyridine, even though they could be good solvents of both guest and host components. Partial solubility in other solvents like dimethyl sulfoxide (DMSO) and sodium hydroxide solutions,<sup>[24,45]</sup> dimethyl acetamide-containing lithium halide<sup>[46,47]</sup> was also reported. Many reactions, modifications, and studies involving PEG/CD PRs have been performed in DMSO as solvent.<sup>[24,47–57]</sup>

Several authors have described a thixotropic viscosity behavior of PRs derived from PEG and  $\alpha$ CDs in DMSO at relatively concentrated solutions.<sup>[44,52,54–56]</sup> This behavior is a consequence of the formation of physical aggregates between PR chains, which are reversibly broken by heating or by the application of a shear. Araki and Ito<sup>[52]</sup> attributed this manner to a combination of intermolecular attractive CD hydrogen bonding and the high rigidity, resulting from relatively high  $\alpha$ CD:PEG inclusion ratios (number of  $\alpha$ CDs per PEG chain) PRs. Travelet et al.<sup>[54]</sup> demonstrated by SANS that these PRs behave like multiblock copolymers in DMSO. One block type consists of a rod-like tube made of 6–7 weakly stacked  $\alpha$ CDs threaded along the PEO chain. The other one is made up of naked polymer segments. In the case of PR/DMSO-concentrated solutions at room temperature, the PR aggregates by forming nanocylinders, which consist of assemblies of  $\alpha$ CD:PEG rod-like tubes resulting from hydrogen-bonding interactions. More recently,<sup>[56]</sup> the same authors studied the PR structure as a function of the temperature and  $\alpha$ CD:PEG ratio in DMSO-concentrated solutions. The behavior of the multiblock copolymers at 43 °C was again observed. When the PR mixtures were cooled down, gelation occurred. The gel structure is due to the formation of regular bundles containing naked PEG segments surrounded by nano-cylinders. Stoichiometry is a crucial parameter controlling the PR prealignment, self-organization (and PR flexibility), which is favored (unfavored) at high  $\alpha$ CDs-to-PEG coverage degrees. Mayumi et al.<sup>[55]</sup> used the same technique to study a PR of PEG ( $\approx 35$  kg mol<sup>-1</sup>) with  $\alpha$ CD of 27% coverage at a lower DMSO concentration regime, and no aggregation was observed. CDs seemed to be distributed randomly along the entire PEG chain in the PR.

In order to clarify the behavior in solution (preferentially DMSO) of this type of PRs, in the present study we report the synthesis and characterization in solu-

tion of some end-capped (with phenoxy or naphthoxy groups) PRs derived from PEG of 3.4, 6.8, and 13.8 kg mol<sup>-1</sup> and native  $\alpha$ -cyclodextrin,  $\alpha$ CD, named PR#:CD:Ph or PR#:CD:Nph (# = 3k, 6k, or 10k) and PRs, where  $\alpha$ CDs were modified with phenylisocyanate,  $\alpha$ CD(PhI), [PR#:CD(PhI):Ph or PR#:CD(PhI):Nph]. For this purpose size exclusion chromatography (SEC/MALS), dynamic light scattering (DLS), and fluorescence techniques were used. In addition, molecular dynamics (MD) simulations on isolated PR chains with different stoichiometries and  $\alpha$ CD orientations, as well as five PR chains placed in a periodic box, were performed to rationalize and explain the experimental behavior and identify the intra- and intermolecular interactions responsible for the PR formation and aggregation.

## 2. Materials, Instrumentation, and Methods

### 2.1. Reagents and Solvents

Dihydroxy-terminated PEG with weight-averaged molecular weights,  $\bar{M}_w$ , of 3.4, 6.8, and 13.8 kg mol<sup>-1</sup> ( $\bar{M}_n$ , of 2.6, 4.8, and 10.2 kg mol<sup>-1</sup>), coded PEG3k, PEG6k, and PEG10k, respectively, were obtained from Fluka and were dried under vacuum at 40 °C prior to using.  $\alpha$ CD was obtained from Wacker-Química Ibérica and was also dried under vacuum at 80 °C. Other reagents and solvents, dichloromethane (CH<sub>2</sub>Cl<sub>2</sub>) (anhydrous, 99.8%), dimethylformamide (DMF) (anhydrous, 99.8%), DMSO (anhydrous, 99.9%), pyridine (99%), *p*-toluenesulfonyl chloride (*p*-TsCl) (98%), 3,5-dimethylphenol (99%), 1-naphthol (Nph) (98%), phenyl isocyanate (PhI) (98%), and triethylamine (Et<sub>3</sub>N) (99.5%), were from Sigma-Aldrich and were used as received. Toluene (99.7%) and sodium hydride (NaH) (55–65% gas volumetric in paraffin oil) were from Fluka. Paraffin oil was rinsed off using *n*-hexane.

For fluorescence experiments, DMSO, methanol (MeOH), and DMF (Aldrich, spectroscopic or HPLC grades, purity  $\geq 99.7\%$ ) were used as solvents. 2-Naphthol and phenol were employed as model compounds for PR fluorescence measurements. DMSO (Aldrich, HPLC grade) and LiBr (Aldrich, purity  $> 99.9\%$ ) were also used for gel-permeation chromatography (GPC) measurements.

### 2.2. Polyrotaxane Synthesis

Two families of PRs based in the above-mentioned PEGs and  $\alpha$ CDs, end-capped with two different bulky groups, 3,5-dimethylphenol (Ph) and 1-naphthol (Nph), respectively, named PR#:CD:Ph and PR#:CD:Nph (# = 3k, 6k, or 10k), were synthesized by using methods well documented in the literature (see brief description and Scheme S1,

Supporting Information).<sup>[19,24,45,58]</sup> A PEG10:Nph, used as reference system, was synthesized following the same procedures as in PRs.

The modification of the previous PRs with phenylisocyanate (PhI), PR#:CD(PhI):Ph, and PR#:CD(PhI):Nph was performed according to procedures published elsewhere (see brief description and Scheme S2, Supporting Information).<sup>[47]</sup> All the products were freeze-dried and kept in vacuum up to their use.

### 2.3. Instrumentation and Methods

<sup>1</sup>H NMR spectra at 500 MHz for all PRs were recorded on a Bruker Avance spectrometer at room temperature. Spectra were measured with four accumulations and 2.18 s for acquisition time. Chemical shifts were referenced to the solvent, DMSO-d<sub>6</sub> ( $\delta = 2.50$  ppm). Fourier Transform IR (FTIR) spectra were recorded from KBr pellets on a Perkin-Elmer GX 2000 (10 scans and 1 cm<sup>-1</sup> resolution). Thermogravimetric analysis (TGA) for all PRs was obtained on a Perkin-Elmer STA 6000 system. After thoroughly drying at 50 °C for 10 min, samples were recorded from 50 to 700 °C at a heating rate of 10 °C min<sup>-1</sup> in a slow nitrogen flow (20 mL min<sup>-1</sup>).

SEC measurements were carried out using equipment that consisted of a pump (Waters, model 510), an injector (Waters, U6K), and two detectors: Optirex Interferometric Refractometer (RI) operating at 632.8 nm and a Dawn DSP-F multiangle light scattering (MALS) photometer, equipped with a He-Ne laser (632.8 nm), both from Wyatt Technology Corp. The chromatographic columns used, Styragel HR 4E, were kept in an oven at 50 °C. The eluent consisted of a  $5 \times 10^{-4}$  M LiBr solution in DMSO that was passed through a 1.0  $\mu$ m cellulose nitrate filter (Whatman) and degassed prior to use. The flow rate was 0.4 mL min<sup>-1</sup>. Repeated injections were made for each sample to ensure the reproducibility of the results. In all cases, the results were reproduced. The light scattering equation and the experimental procedure used to collect and process SEC/MALS data in order to obtain molecular weights were explained elsewhere.<sup>[59-61]</sup> The value of  $dn/dc$  for PRs in DMSO was measured in batch with the RI detector by using solutions of PR10:CD:Nph at different concentrations. The value obtained was 0.055 mL g<sup>-1</sup>, which is rather similar to the one reported<sup>[62]</sup> for PRs from PEG and  $\alpha$ CDs in the same solvent.

DLS measurements were performed using a Malvern Zetasizer Nano Series operating a 4 mW He-Ne laser at 633 nm. Analysis was performed in DMSO, at an angle of 173° and different temperatures, using 1 cm glass cuvettes.

Absorption spectra were recorded in a Lambda 35 Perkin Elmer UV-vis spectrophotometer. Steady-state and time-resolved fluorescence measurements were

performed on SLM 8100C Aminco and FL900 Edinburgh Instruments spectrofluorometers, respectively. Decay intensity profiles were fitted to a sum of exponential decay functions  $I(t) = \sum_{i=1}^n A_i e^{-t/\tau_i}$  by the iterative reconvolution method.<sup>[63]</sup> The average lifetime of a multiple-exponential decay function was then defined as  $\langle \tau \rangle = \sum_{i=1}^n A_i \tau_i^2 / \sum_{i=1}^n A_i \tau_i$ , where  $A_i$  is the pre-exponential factor of the component with a lifetime  $\tau_i$  of the multi-exponential function intensity decay.<sup>[64]</sup> More details are included in the Supporting Information.

MD simulations were computed using Sybyl-X1.2<sup>[65]</sup> and the Tripos force field.<sup>[66]</sup> Trajectories were performed on several isolated PRs named PR3:HTCD<sub>n</sub>:Ph and PR3:HTCD<sub>n</sub>:Ph that were composed of: a) a 3k molecular weight Ph-end-labelled PEG chain (68 ethylene oxide units), which were initially placed in the all trans-conformation and b) a molecular channel that contains  $n$  ( $= 2, 4, 12, 14, 16, \text{ or } 20$ ) non-distorted HH- or HT-oriented  $\alpha$ CDs. These  $\alpha$ CDs were initially located uniformly and symmetrically distributed from the center of mass of the *trans*-PEG chain and their centers of mass were separated from each other by  $\approx 8$  Å. Figure S1 in the Supporting Information depicts an example of both types of PR configurations studied.

The potential energy was obtained as the sum of bond stretching, angle bending, torsional, van der Waals, electrostatics, and out-of-plane contributions. Charges were calculated for each repetitive unit and terminal group using MOPAC (AM1).<sup>[67]</sup> CD charges were those used previously by us.<sup>[68]</sup> A relative permittivity  $\epsilon = 3.5$  was utilized in the vacuum.<sup>[27]</sup> The simulations were started on minimized PR structures by using the simplex algorithm and the conjugate gradient (0.15 kcal mol<sup>-1</sup> Å<sup>-1</sup>) termination method.<sup>[69,70]</sup>

Each 3 ns MD simulation was started at 1 K and the temperature was increased at intervals of 10 degrees remaining in the intermediate states 300 fs until reaching the temperature of interest of 500 K. Vibrations for bonds connecting hydrogen atoms were eliminated. Integration time was 2 fs and images were collected every 200 fs, providing 15 000 conformations for each trajectory. The high temperature of 500 K allows for a broad sampling of the conformational space during the 3.0 ns MD trajectories.

The number of intra- and intermolecular hydrogen bonds (HBs) of the systems were obtained by assuming the presence of a HB, when the acceptor and hydrogen bonded to a donor are separated by a distance in the 0.8–2.8 Å interval and the angle formed by O...H–O ranges from 120° to 180°.

To evaluate the intermolecular PR interactions, five PR3:HHCD<sub>20</sub>:Ph PR chains were randomly distributed in a periodic boundary conditions (PBC) box of dimensions 27.6 nm  $\times$  19.5 nm  $\times$  19.5 nm and then a 1 ns MD

Table 1. Molecular weight and composition of end-capped with 3,5-dimethylphenol and 1-naphthol polyrotaxanes.

Polyrotaxane	Number of CD per chain <sup>a)</sup>	Coverage <sup>b)</sup> [%]	EG/CD molar ratio <sup>c)</sup>	$\bar{M}_n$ <sup>d)</sup> [g mol <sup>-1</sup> ]
PR3:CD:Ph	19	74	3.1	21 000
PR6:CD:Ph	33	70	3.3	37 000
PR10:CD:Ph	39	39	5.9	48 000
PR3:CD:Nph	16	62	3.7	18 000
PR6:CD:Nph	29	61	3.8	33 000
PR10:CD:Nph	41	41	5.7	50 000

<sup>a)</sup>Number of  $\alpha$ CDs per chain, calculated by <sup>1</sup>H NMR spectroscopy; <sup>b)</sup>A molar ratio of 2.3 ethylene glycol (EG) repeat units per CD means a 100% coverage;<sup>[24]</sup> <sup>c)</sup>The molar ratio that shows the EG units shared for each  $\alpha$ CD; <sup>d)</sup>Number-averaged molecular weight obtained from the <sup>1</sup>H NMR spectroscopy analysis of the PEG ( $\delta = 3.51$  ppm) and  $\alpha$ CD ( $\delta = 4.80$  ppm) proton signals<sup>[24,71]</sup>; The values of the initial PEG  $\bar{M}_n$  were 2.6, 4.8, and 10.2 kg mol<sup>-1</sup>.

trajectory, following similar protocols as for each isolated PR, was simulated.

## 2.4. Polyrotaxanes Characterization

The composition for the non-modified PRs was obtained by <sup>1</sup>H NMR spectroscopy. (Figure S2, Supporting Information). The  $\alpha$ CD/PEG molar ratios were estimated by comparison of  $\alpha$ CD C(1)-H ( $\delta = 4.80$  ppm) and PEG ( $\delta = 3.51$  ppm) proton signals as described elsewhere.<sup>[24,71]</sup> Table 1 summarizes the stoichiometry ratios for the PRs. The PEG chain covered by CDs (percentage of coverage) was also obtained under the assumption that a PEG chain is saturated with CDs, when the molar PEG:CD fraction is 2.3:1.<sup>[24,58]</sup> As collected in Table 1, the percentage of coverage (EG/CD molar ratios) for non-modified PRs decreases (increases) with PEG molecular weight, but the values obtained for PRs with small-PEG chains, 3k and 6k, are significantly higher (lower) than that for the 10k ones in both series. The results are in good agreement with those obtained by Zhao and Beckham.<sup>[58]</sup> Nevertheless, for checking purposes, the number of CDs per PR was also estimated from the  $2I_{1H}/I_{mH}$  ratios, where  $I_{1H}$  and  $I_{mH}$  are the integrated areas under the  $\alpha$ CD C(1)-H ( $\delta = 4.80$  ppm) and the methyls from the PEG terminal Ph groups ( $\delta = 2.22$  ppm), respectively.<sup>[58]</sup> No relevant stoichiometric differences were obtained with this method and the previous one.<sup>[24,58,71]</sup> Unfortunately, NMR spectroscopy signals are too small to obtain any reliable results for PRs derived from the largest molecular-weight PEG (10k). As collected in Table 1, the use of Nph or Ph stoppers does not imply significant stoichiometry changes. The number-averaged molecular weights for non-modified PRs, estimated from the <sup>1</sup>H NMR spectroscopy analysis of the PEG ( $\delta = 3.51$  ppm) and  $\alpha$ CD ( $\delta = 4.80$  ppm) proton signals,<sup>[24]</sup> are depicted in the last column of Table 1.

<sup>1</sup>H NMR spectra for PRs modified with phenylisocyanate, PR#:CD(PhI):Ph and PR#:CD(PhI):Nph, showed the carbamate ( $\delta = 9.66$  ppm) and phenylisocyanate aromatic

( $\delta = 7.46, 7.18, 6.92$  ppm) signals (Figure S3, Supporting Information). The complete interpretation of the <sup>1</sup>H NMR spectroscopy of all modified PRs was difficult because of the small intensity of the anomeric peaks from  $\alpha$ CD.

Assignments of bands in the FTIR spectra for the PRs (Figure S4, Supporting Information) agreed with the proposed structures. Moreover, the lack of a signal at 2267 cm<sup>-1</sup> confirms the absence of free phenylisocyanate in all the modified PRs.<sup>[72]</sup>

The thermogravimetric analysis (TGA) was also performed on all the PR samples. Figure 1 shows the thermograms for the four PRs derived from PEG10k, together with that for  $\alpha$ CD. No weight loss was detected in the 50–184 °C temperature range for any of the non-modified PRs. First, free  $\alpha$ CD showed a slow decrease in weight at 50 °C having approximately 95% in weight left at 122 °C. Subsequently,  $\alpha$ CD showed a rapid decrease in weight over 280 °C with approximately 18% in weight left as residue at 430 °C. TGA of non-modified PRs showed a one-stage weight-loss pattern that corresponded to the

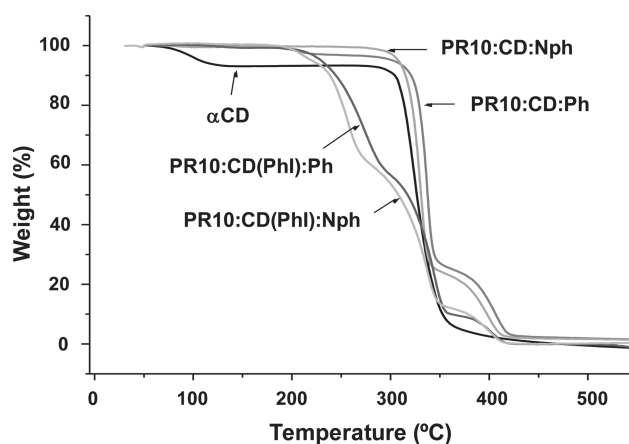


Figure 1. Thermogravimetric analysis for  $\alpha$ CD and PRs based in PEG10k.



degradation of the  $\alpha$ CD and PEG moieties that occurred at the temperature ranges of 275–359 °C.<sup>[19,42,73]</sup> Although the thermogram of the PEG chain was not shown in the figure, the degradation of the PEG chain occurred at the temperature ranges of 168–350 °C. Thus, the CD stabilizes the PEG chains in all PRs because the degradation of all PRs starts 100 °C after the PEG degradation.

The TGA profiles of the modified phenylcarbamate PRs with end-bulky Nph or Ph groups, PR#:CD(PhI):Nph and PR#:CD(PhI):Ph, were very similar to the TGA curves that are well referenced in the literature for other polymers, such as polyurethanes<sup>[74]</sup> and cellulose carbamates.<sup>[72,75,76]</sup> They present a three-stage weight-loss pattern consisting of the degradation of the PhI,  $\alpha$ CD, and PEG components in the 180–260, 260–360, and 360–420 °C temperature ranges, respectively. The first stage reflects the percentage of phenylcarbamate anchored to the  $\alpha$ CD and involves two substages. In the first one (ca. 180–220 °C), the thermal cleavage of the urethane bond, which dissociates into the starting components phenylisocyanate and hydroxyl group of the CD, takes place.<sup>[74,75]</sup> The second substage (220–260 °C) is due to the degradation of the phenylisocyanate regenerated in the first substage and it can be used to calculate the percentage of phenylisocyanate groups in the CDs.<sup>[75]</sup> The results, collected in the second column of Table 2, indicate that roughly one-third of hydroxyl groups were substituted.

### 3. Results and Discussion

#### 3.1. Size Exclusion Chromatography (SEC-MALS)

The upper panel of Figure 2 depicts the chromatograms through the RI signals (broken lines) and one of the MALS signals at 90° (solid lines) for the different PRs. The light scattering signals are proportional to the product of molecular weight and concentration and they obviously have a different shape than the RI signals, which are proportional

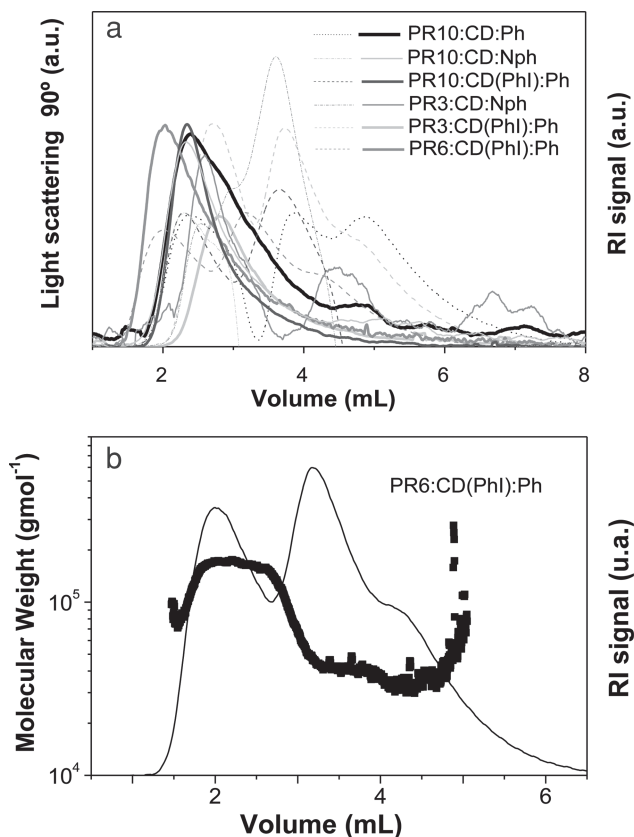


Figure 2. a) Chromatogram traces of some PRs in DMSO. Light scattering, MALS, signals (solid lines), and refractive index, RI, signals (broken lines) plotted versus elution volume. b) Molecular weight (filled squares) and RI signal (solid line) versus elution volume for PEG6:CD(PhI):Ph.

to the concentration. Chromatograms are multimodal and are formed by the overlapping of several narrower peaks, RI traces show two well-defined peaks, and in some cases, a shoulder at high elution volumes. We do not have any conclusive explanation for this shoulder. However, the molecular weights are close to those obtained for the second peak and, in all samples, they are higher than molecular weights of free PEG chains.

The MALS detector permits the determination of the molecular weight of the species in solution as they elute the columns, and the bottom of Figure 2 displays the molecular weight dependence on elution volume superimposed on the chromatogram trace (RI signal) for PR6:CD(PhI):Ph as an example. The accuracy of the molecular weight decreases with increasing elution volumes, thus the determination of the lower molecular weights that appear at the end of the chromatograms is less precise. Nevertheless, Figure 2b clearly shows that molecular weight diminishes as the elution volume increases, as expected. However, the decrease is very mild (i.e., the molecular weight remains approximately constant) for each one of the first two peaks

Table 2. Percentage of substitution of phenylisocyanate per polyrotaxane and hydroxyl group respectively, obtained by TGA.

Polyrotaxane	PhI weight in PR [%]	Substituted hydroxyl groups [%]	$\bar{M}_n$ [g mol <sup>-1</sup> ]
PR3:CD(PhI):Ph	32	24.3	31 000
PR6:CD(PhI):Ph	39	33.5	61 000
PR10:CD(PhI):Ph	31	25.5	70 000
PR3:CD(PhI):Nph	36	29.5	28 000
PR6:CD(PhI):Nph	37	31.2	52 000
PR10:CD(PhI):Nph	34	29.3	76 000

Table 3. Weight-averaged molecular weight for the two chromatogram peaks of PRs and ratio between molecular weights of first peak and isolated PR chain.

Polyrotaxane	$\bar{M}_w$ [g mol <sup>-1</sup> ]		M(first peak)/M(PR chain)
	First peak	Second peak	
PR3:CD(PhI):Ph	106 000	31 000	3.0
PR6:CD(PhI):Ph	169 000	41 000	2.6
PR10:CD(PhI):Ph	276 000	40 000	3.7
PR10:CD:Ph	105 000	22 000	2.3
PR10:CD:Nph	96 000	–	2.1

that form the chromatogram but there is an abrupt change between them. The molecular weight dependence of the remaining PRs behaves in a similar manner. The molecular weight of the PR3:CD:Nph was difficult to obtain because its solution in DMSO was reddish.

Weight-average molecular weights,  $\bar{M}_w$ , for the PRs are displayed in Table 3. For the PR10:CD:Nph, the RI signal has two overlapped peaks whose separation is not enough to determine the molar mass of the second peak (see last row of Table 3). The molecular weights of the first peak of the chromatograms are too large to correspond to isolated chains of PRs since they are two to three times their expected values calculated from NMR spectroscopy and TGA data (Table 1 and 2). Thus, this peak suggests that aggregation among PR chains occurs. The molecular weights of the second peak, collected in Table 3, are much closer to the ones estimated from NMR spectroscopy data (Table 1 and 2) and thus, they might be attributed to isolated PR chains. The differences among them are due to the fact that the samples are polydisperse and the chromatographic separation between aggregates and isolated chains is not complete, as can be seen in Figure 2. Information about the aggregates can be inferred from the molecular weights of the first peak and their relationship with those of isolated chains. The molecular weights of the aggregates increase as the PEG size increases, as can be noticed for PR#CD(PhI):Ph in Table 3, whereas the ratio between the molecular weight of the aggregate and the molecular weight of the corresponding PR chain (fourth column of Table 3) for the three PRs is fairly constant. Thus, the polymer forms aggregates in DMSO with a number of chains that seem not to depend on the size of the PEG. When comparing molecular weights for the three PRs derived from PEG10k, it was first observed that the type of end groups, Ph or Nph, has no influence on the molecular weight and second, that the superficial modification in the CD seems to favor the aggregation, increasing the number of chains in the aggregate. The aggregation of PRs derived from PEG and  $\alpha$ CDs in DMSO has been described

in the literature, as well as earlier in this paper, and depends on the  $\alpha$ CDs-to-PEG coverage, solution concentration, and temperature.<sup>[44,52,54–56]</sup>

### 3.2. Dynamic Light Scattering

DLS measurements of PR10:CD:Nph (35% CD coverage) solutions in DMSO at  $\approx 2.4$  mg mL<sup>-1</sup> (similar concentration as SEC measurements) were carried out at three different temperatures, 25, 50, and 75 °C. The intensity distribution at 50 °C (the temperature used in SEC/MALS) showed two broad peaks at an apparent hydrodynamic radius of  $9 \pm 3$  and  $80 \pm 40$  nm. These results are in good agreement with the aggregation behavior found in both SEC/MALS. These two distinct peaks also appear at 25 °C with a similar broadness, although they are slightly displaced toward larger sizes. At 75 °C, the aggregate peak is clearly shifted toward smaller values of approximately  $30 \pm 20$  nm and the second peak appears at ca. 2 nm. This fact would indicate that the temperature rise opposes the aggregation and thus the size of the aggregates diminishes, as one could expect and as was described by several authors.<sup>[44,52,54–56]</sup> After the data acquisition at 75 °C, the PR solution was cooled right back to 25 °C. The intensity distribution profiles of the cooled solution were similar to those previously collected at this temperature, indicating that aggregation in DMSO is a reversible process. Although the DLS measurements must be handled cautiously due to the polydispersity of the samples, they support the aggregation behavior of PRs.

### 3.3. Fluorescence

As depicted in Figure 3a, the fluorescence spectrum of a dilute solution of the naphthyl (Nph) end-labelled PEG chain (PEG10:Nph) in DMSO upon excitation of naphthalene moiety (295 nm) showed: i) a typical monomer emission band ( $\approx 340$  nm), similar to the one observed for 2-naphthol model; ii) an excimer band ( $\approx 425$  nm) due to intramolecular end-to-end group interactions. Figure 3a also depicts emission spectra for PR10:CD:Nph and PR3:CD:Nph, which only exhibited the single monomer band. The absence of an excimer band is a consequence of the formation of relatively extended conformations for the PEG immersed in the  $\alpha$ CDs channel, which hinders the conformations where both end groups come close together. This did not occur for the PEG free polymer chain (i.e., PEG10:Nph).

Figure 3 (right) shows fluorescence emission spectra for DMSO dilute solutions of phenol (Ph) model and PRs containing 3,5-dimethylphenoxide (Ph) end groups, either with unmodified (native)  $\alpha$ CDs (PR#:CD:Ph) or modified

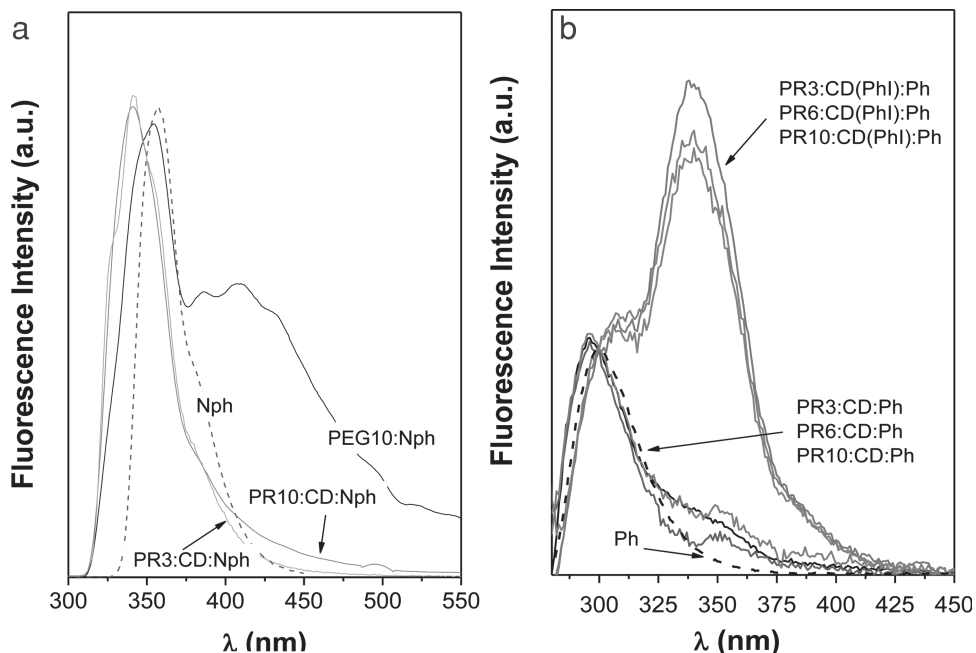


Figure 3. Emission spectra for DMSO dilute solutions of (a) 2-naphthol (Nph), PEG10:Nph and two end-labelled PRs with Nph groups at 25 °C and (b) phenyl end-labelled PR#:CD:Ph and PR#:CD(PhI):Ph PRs at the same experimental conditions.

ones with PhI groups, PR#:CD(PhI):Ph, upon excitation of 275 nm. Spectra for PR#:CD:Ph, regardless of molecular weight, show features similar to those naphthalene end-labelled PRs (PR#:CD:Nph), exhibiting a single-Ph end-group monomer band, centered now at  $\approx 295$  nm. PR#:CD(PhI):Ph, however, showed an additional excimer band, whose maximum is placed around 425 nm. As the PR concentration was very low and its change did not affect the excimer-to-monomer ratios and presumably, as for PR#:CD:Ph, end-to-end excimers are quite unlikely, the latter emission was attributed either to interactions between PhI groups within each CD(PhI) or between adjacent CD(PhI)s in the PR, or probably to both. Whatever the solvent used, no excimers were observed for the PR#:CD:Ph (and PR#:CD:Nph) series. However, the PR#:CD(PhI):Ph series always exhibits excimer emission bands, whose intensity depends on the solvent nature but not on the PR molecular weight. This reinforces the idea that short-range phenyl group interactions from CD(PhI)s are involved. Table S1 in the Supporting Information collects the excimer-to-monomer intensity ratios for Ph end-labelled PRs in different solvents.

Emission spectra (Figure S5, Supporting Information) for PEG10:Nph and PR10:CD:Nph solutions of DMSO/EtOH mixtures by keeping polymer concentration constants at ( $0.016 \times 10^{-3}$  M) upon excitation of the Nph chromophore were also recorded. Results for PEG10:Nph show an increase in the fluorescence intensity upon increasing the EtOH content (solvent polarity decreasing), which is also accompanied by a slight decrease of the

excimer-to-monomer ratios. PR10:CD:Nph and the Nph model compound, which obviously do not display excimer bands, exhibit the opposite behavior, an emission decreasing with the EtOH content. This may indicate that Nph end groups in the PR10:CD:Nph behave like the model compound in each solvent. Nph groups in PR10:CD:Nph are more exposed to the solvent than the same groups in the PEG10:Nph.

Weighted average lifetimes  $\langle \tau \rangle$  for PEG10:Nph and PR10:CD:Nph solutions in DMSO/EtOH mixtures at 25 °C were also obtained from analysis of the fluorescence intensity decays ( $\lambda_{em} = 340$  nm). Decay intensity profiles were bi-exponential with components around 2–3 ns (5–7 ns) and 7–8 ns (8–10 ns) for PEG10:Nph (PR10:CD:Nph). As a consequence,  $\langle \tau \rangle$  was always shorter for PEG10:Nph than for PR10:CD:Nph dilute solutions, probably because monomer emission is quenched by excimer formation.  $\langle \tau \rangle$  values for PR10:CD:Nph, whose end groups are more exposed to the solvent, decrease with ethanol content from 9.8 ns (DMSO) to 7.7 ns (40% DMSO/EtOH), whereas for the different PEG10k:Nph solutions, whose chromophores are apparently more shielded from the solvent, the remaining constant  $\approx 6.7$  ns hardly changes at the same temperature.

With the purpose of reinforcing the experimental findings on the presence of the PR aggregation, the intermolecular phenol to naphthol energy transfer efficiency  $\Phi_{ET}$ , was evaluated for an equimolar PR10:CD:Ph and PR10:CD:Nph ( $0.14 \times 10^{-3}$  M each) mixture in DMSO at 25 °C. The efficiency was defined as:<sup>[77]</sup>



$$\frac{\Phi_{\text{ET}}}{1 - \Phi_{\text{ET}}} = \frac{\phi_{\text{D}} I_{\text{A}}}{\phi_{\text{A}} I_{\text{D}}} \quad (1)$$

where  $\phi_{\text{D}}$  and  $\phi_{\text{A}}$  are the fluorescence quantum yields<sup>[78]</sup> for individual PR10:CD:Ph ( $0.14 \times 10^{-3}$  M) and PR10:CD:Nph ( $0.14 \times 10^{-3}$  M) DMSO dilute solutions upon excitation, both at 270 nm.  $I_{\text{A}}$  and  $I_{\text{D}}$  are the integrated areas under the emission Nph and Ph bands, respectively, obtained for the equimolar mixture upon the same excitation wavelength. The emission spectra for PR10:CD:Ph and PR10:CD:Nph and the mixture in DMSO at 25 °C are depicted in Figure S6 in the Supporting Information.

Equation 1 provides  $\Phi_{\text{ET}} = 0.45$ . The Förster radius for the Ph-to-Nph transfer is around 1.6 nm.<sup>[79]</sup> At the concentrations used ( $\approx 0.14 \times 10^{-3}$  M), a simple calculation of the average of the distances between chromophores gives a value of around 15 nm. At this distance, ten times larger than Förster radius, the efficiency for Ph-to-Nph energy transfer should be zero. The large efficiency can only be explained under the assumption that the PRs in DMSO solution aggregate.

### 3.4. Circular Dichroism

PR#:CD:Ph and PR#:CD:Nph in DMSO at 25 °C, which only contain Ph or Nph terminal groups, respectively, hardly exhibited any induced circular (ICD) dichroism signal. The ICD signal, if it appeared, could be attributed to the possible interaction of Ph or Nph chromophores with the closest CD quiral macrorings located at both ends of the channel. The absence might presumably be a consequence of the low CD coverage of the PRs studied. PR#:CD(Phl):Ph, however, showed a negative spectrum in the 260–280 nm absorption range, which was attributed to the quirkality of the CD(Phl) itself.

### 3.5. Molecular Dynamics Simulations

End-to-end distances, root-mean-square radius of gyration, and PEG–CD and CD–CD per CD unit interaction energy averages obtained from analysis of the 3 ns MD trajectories for PEG3:Ph and PR3:CD<sub>*n*</sub>:Ph ( $n = 2, 4, 8, 12, 14, 16,$  and 20) containing HH- or HT-oriented CDs are collected in Table S2 in the Supporting Information. In agreement with the fluorescence spectra, the average of the distances between the center of mass of terminal Ph groups for any of the PRs studied are larger than the minimum requirements for the formation of intramolecular excimers.<sup>[80]</sup> For the end-labelled PEG chain, PEG3:Ph, these averages are also larger than those expected for a PEG chain that, as experimentally observed, exhibited fluorescence emission from intramolecular excimers. Nevertheless, histories of the distances between the center of mass of Ph end groups

(Figure S7, Supporting Information), reveal that PEG3:Ph can adopt, during the trajectory, conformations where Ph groups are close together and capable of forming intramolecular excimers. As stated before, Ph–Ph distances for any of the PR3:CD<sub>*n*</sub>:Ph studied are relatively large to form excimers, but too short if compared with the distance obtained for the all trans-conformation of a PEG3k chain ( $\approx 24.5$  nm). According to some MD calculations reported by us,<sup>[27]</sup> the end-to-end distances for a totally saturated PEG3k (100% coverage), containing a population of trans states for all the torsional angles of the oxyethylene units in the 80–90% range, was approximately 23 nm.

In addition, PEG–CD interaction energies, whatever the CD orientations (HH or HT) were, showed a stabilization of the system upon the increasing of  $n$ . Furthermore, the interaction of each CD bonded with its neighbor, measured as CD–CD/ $n$  energy interaction, contributed favorably to the formation of PRs, becoming more negative as  $n$  increased. This interaction was more favorable for HH-oriented PRs than HT ones. Harada et al.<sup>[26,81]</sup> attributed this stabilization to the presence of intermolecular CD–CD hydrogen bonds, which are more numerous for HH sequences. However, the calculated PEG–CD-binding energies also favored the HH sequences over the HT ones by 3–8%. According to these calculations, the PEG might stabilize by capturing as many CDs as its length permits. However, for the PRs used in our experiments the PEG chains were not saturated by CDs. Entropic effects obviously played an important role in PR formation. The mean-square radius of gyration  $\langle s^2 \rangle^{1/2}$  for PRs was in the 11–22 Å range and it evidently increased with  $n$ . Comparison of the values for HH and HT PRs, resulted in larger values for the HT ones, most likely attributed to the less effective CD–CD and PEG–CDs interactions obtained for HT CD-oriented PRs as compared with the HH ones. Unfortunately,  $\langle s^2 \rangle^{1/2}$  can only be obtained by SEC/MALS from the angular dependence of scattered light, when the polymer sizes exceed the  $\lambda/20$  value of the wavelength of incident radiation in order to notice this angular dependence. Apparently, this is not the case with this PR series.

The average of the distances ( $d$ ) between the center of mass of adjacent CD units for HH- and HT-oriented PRs containing 16 and 20 PEG units were calculated (Table S3, Supporting Information). Two quite distinguishable ( $d$ ) values were obtained. The first one with ( $d$ ) < 11–12 Å, which correspond to nearly parallel adjacent CD pairs; and a second one with ( $d$ ) > 12–13 Å. The last distance also corresponds to neighbor CDs between which, the PEG chain folds back producing a reversal in the direction of the PR chain (hairpin). Then, both portions of the PR stand nearly parallel with CD of each branch laterally interacting. In fact these interactions, to which HB between CDs presumably contribute, are responsible for the stabilization of the folded structure.

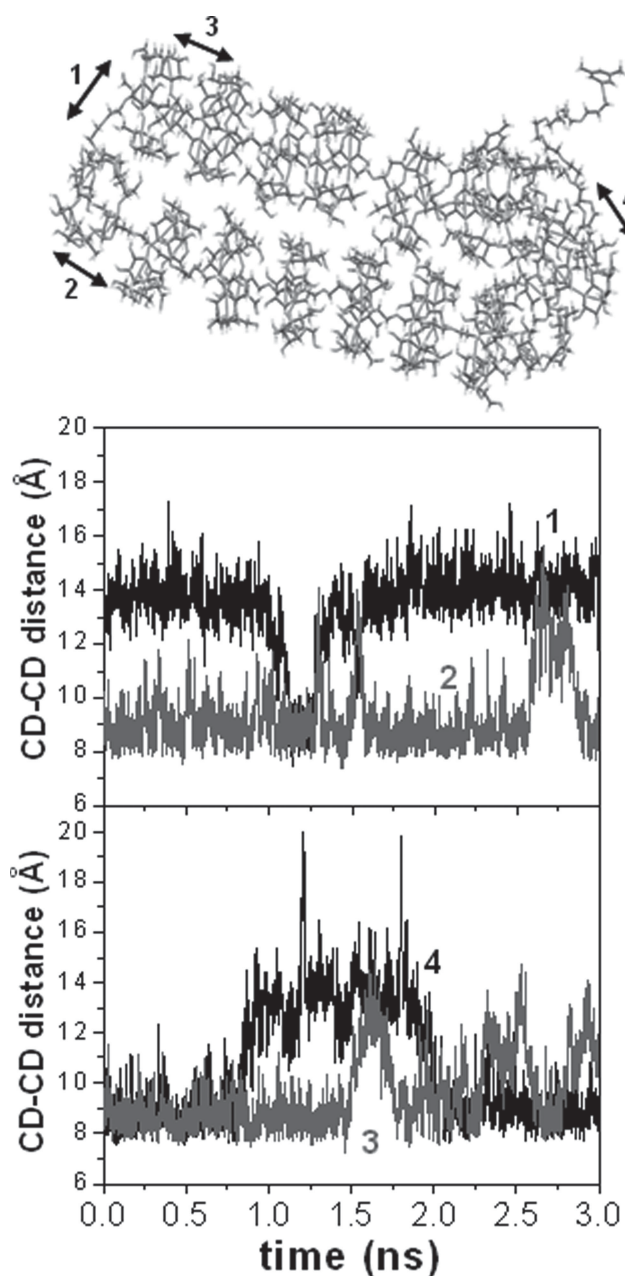


Figure 4. Histories of distances between the center of mass of some pairs of adjacent CDs obtained from the analysis of the 3 ns MD trajectories for PR<sub>3</sub>:HTCD<sub>16</sub>:Ph. A snapshot of the PR trajectory (time = 0.2 ns) is superimposed, showing the distances whose histories are represented.

Figure 4 shows the histories during the MD trajectory for the distances between the center of mass of some CD pairs for PR<sub>3</sub>CD<sub>16</sub>HT. The larger distance, as depicted in the superimposed figure, is responsible for the hairpin in the PR chain. A simple calculation of the number of intermolecular HBs between CDs of both PR portions at both sides of the hairpin for PR<sub>3</sub>CD<sub>16</sub>HT provides an average of  $4.4 \pm 2.3$  HBs from the 15 000 conformations.

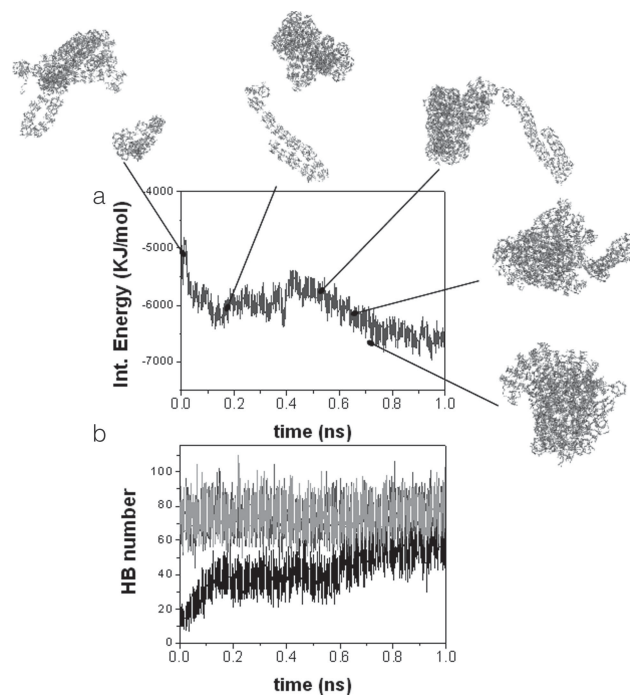


Figure 5. Histories of (a) binding energies per PR unit and (b) number of intermolecular hydrogen bonds (HBs) between PR chains (in black) and intramolecular ones for two individual PR chains obtained from the analysis of the 1 ns MD trajectory for five PR<sub>3</sub>:HHCD<sub>16</sub>:Ph chains in a periodic box. The structures of the system at different times are superimposed.

Nevertheless, some of them have a maximum of 16 of these HB interactions. The number of hairpins does not depend on the HT or HH CD orientation. The presence of hairpins makes the dimensions of the unsaturated PR decrease considerably. Loethen et al.<sup>[82]</sup> reported AFM images for a PEG (1500 kg mol<sup>-1</sup>) with  $\alpha$ CD PRs evaporated from DMSO, indicating the presence of uniformly distributed topographical features that correspond to: i) fully threaded PEG with  $\alpha$ CD PR ( $\approx 13.4$  nm length); ii) structures of  $\approx 8$  nm resulting from the partially threaded linear PR containing hairpins, and iii) larger species from the presence of aggregates of PRs.

Aggregation was also investigated from analysis of the 1 ns MD trajectory of five PR<sub>3</sub>:HHCD<sub>20</sub>:Ph chains, which initially were randomly distributed in a PBC box. Undoubtedly the results, as Figure 5 depicts, prove that portions of each single PR chain tend to self-associate intra-molecularly through the formation of hairpins, where portions of the chain interact side by side and where HB interactions contribute to the stabilization. Moreover, PRs tend to spontaneously aggregate in the vacuum and this association is accompanied by favorable attractive intermolecular interactions between PRs. Whereas the number of total intramolecular HBs in the PR chains keeps almost constant during the entire MD

trajectory, the number of HBs between CDs from different PR chains increases upon association contributing to the aggregate stabilization as shown in Figure 5. These results are in good agreement with the behavior found by SEC/MALS, DLS, and fluorescence techniques.

## 4. Conclusion

The SEC/MALS technique allows us to obtain the molecular weight distributions and stoichiometries (4–17 ethylene oxide units per CD) of several PRs, which seem to aggregate in DMSO solution. Whereas the PR aggregation does not seem to depend on the size of the PEG chain and the type of anchored end groups, the superficial modification of CD with phenylisocyanate increases the aggregation numbers. PR aggregation decreases with temperature and it seems to be a reversible process. The absence of intramolecular excimers for phenyl- or naphthyl-end-labelled PRs infers that they adopt relatively extended conformations (at least more than the free PEG chain). The relatively high intermolecular energy transfer efficiency between Ph and Nph chromophores from the end groups of PR chains also agrees with the presence of aggregates in solution. MD calculations prove that CD–PEG and CD–CD (per CD unit) energy interactions are attractive, both increasing with the CD content. HH sequences are more favorable than HT ones. The presence of hairpins in the (non-saturated) PR chains contributes to lowering their expectedly large dimensions. Calculations also infer that PR chains spontaneously aggregate. The process is accompanied by an increase in the number of hydrogen bonds between CDs of different PR chains. Interaction energies are also favorable to aggregation.

## Acknowledgements:

This work was supported by the University of Alcalá (GC2011–002 and UAH2011/EXP-036) and Nanomod (MAT2010–17091) from the Spanish Ministerio de Ciencia e Innovación. The authors acknowledge the assistance of M. L. Heijnen with the preparation of the manuscript.

## References

- [1] L. Brunsveld, B. J. B. Folmer, E. W. Meijer, R. P. Sijbesma, *Chem. Rev.* **2001**, *101*, 4071.
- [2] J.-M. Lehn, *Polym. Int.* **2000**, *51*, 825.
- [3] W. H. Binder, R. Zirbs, *Adv. Polym. Sci.* **2007**, *207*, 1.
- [4] A. Harada, *Supramolecular Polymer Chemistry*, Wiley-VCH Verlag GmbH & Co. KGaA, Weinheim, Germany **2012**, p. 372
- [5] A. Harada, *Acc. Chem. Res.* **2001**, *34*, 456.
- [6] T. Takata, N. Kihara, Y. Furusho, *Adv. Polym. Sci.* **2004**, *171*, 1.
- [7] A. Harada, A. Hashidzume, Y. Takashima, *Adv. Polym. Sci.* **2006**, *201*, 1.
- [8] J. Araki, K. Ito, *Soft Matter* **2007**, *3*, 1456.
- [9] A. Harada, A. Hashidzume, H. Yamaguchi, Y. Takashima, *Chem. Rev.* **2009**, *109*, 5974.
- [10] S. A. Nepogodiev, J. F. Stoddart, *Chem. Rev.* **1998**, *98*, 1959.
- [11] In *Comprehensive Supramolecular Chemistry: Cyclodextrins*, Vol. 3, (Eds: J. Szejtli, T. Osa), Pergamon, Oxford, UK **1996**, p. 693.
- [12] V. T. D'Souza, K. B. Lipkowitz, *Chem. Rev.* **1998**, *98*, 1741.
- [13] E. Engeldinger, D. Armspach, D. Matt, *Chem. Rev.* **2003**, *103*, 4147.
- [14] A. Douhal, *Cyclodextrins Materials Photochemistry, Photo-physics and Photobiology*, Elsevier, Amsterdam **2006**.
- [15] H. Dodziuk, *Cyclodextrins and Their Complexes: Chemistry, Analytical Methods, Applications*, Wiley-VCH Verlag GmbH & Co. KGaA, Weinheim, Germany **2008**, p. 489 .
- [16] F. Davis, S. Higson, *Macrocycles: Construction, Chemistry and Nanotechnology Applications*, John Wiley & Sons, Chichester, UK **2011**.
- [17] A. Harada, M. Kamachi, *Macromolecules* **1990**, *23*, 2821.
- [18] G. Wenz, B. Keller, *Angew. Chem.* **1992**, *104*, 201.
- [19] A. Harada, J. Li, M. Kamachi, *Macromolecules* **1993**, *26*, 5698.
- [20] A. Harada, *Carbohydr. Polym.* **1997**, *34*, 183.
- [21] J. Li, A. Harada, M. Kamachi, *Polym. J.* **1994**, *26*, 1019.
- [22] A. Harada, J. Li, M. Kamachi, *Macromolecules* **1994**, *27*, 4538.
- [23] K. A. Udachin, L. D. Wilson, J. A. Ripmeester, *J. Am. Chem. Soc.* **2000**, *122*, 12375.
- [24] A. Harada, J. Li, M. Kamachi, *J. Am. Chem. Soc.* **1994**, *116*, 3192.
- [25] A. Harada, H. Yamaguchi, in *Synthesis of Polymers: New Structures and Methods*, (Eds: D. A. Schlüter, C. Hawker, J. Sakamoto), John Wiley & Sons, New York **2012**, p. 1113.
- [26] A. Harada, J. Li, M. Kamachi, *Nature* **1992**, *356*, 325.
- [27] J. Pozuelo, F. Mendicuti, W. L. Mattice, *Macromolecules* **1997**, *30*, 3685.
- [28] A. Harada, J. Li, M. Kamachi, *Nature* **1993**, *364*, 516.
- [29] S. Samitsu, J. Araki, T. Shimomura, K. Ito, *Macromolecules* **2008**, *41*, 5385.
- [30] T. Ooya, N. Yui, *J. Controlled Release* **2002**, *80*, 219.
- [31] N. Yui, T. Ooya, *Chem. Eur. J.* **2006**, *12*, 6730.
- [32] T. Shimomura, T. Akai, T. Abe, K. Ito, *J. Chem. Phys.* **2002**, *116*, 1753.
- [33] T. Akai, T. Shimomura, K. Ito, *Synth. Met.* **2003**, *135–136*, 777.
- [34] A. Farcas, M. Grigoras, *J. Optoelectron. Adv. Mater.* **2000**, *2*, 525.
- [35] A. Farcas, E. G. Hitruc, *Dig. J. Nanomater Bios.* **2011**, *6*, 1649.
- [36] A. Farcas, A.-M. Resmerita, A. Stefanache, M. Balan, V. Harabagiu, *J. Org. Chem.* **2012**, *8*, 1505.
- [37] J. Araki, T. Kataoka, N. Katsuyama, A. Teramoto, K. Ito, K. Abe, *Polymer* **2006**, *47*, 8241.
- [38] Y. Okumura, K. Ito, *Adv. Mater.* **2001**, *13*, 485.
- [39] G. Fleury, G. Schlatter, C. Brochon, G. Hadziioannou, *Polymer* **2005**, *46*, 8494.
- [40] G. Fleury, G. Schlatter, C. Brochon, G. Hadziioannou, *Adv. Mater.* **2006**, *18*, 2847.

- [41] G. Fleury, G. Schlatter, C. Brochon, C. Travelet, A. Lapp, P. Lindner, G. Hadziioannou, *Macromolecules* **2007**, *40*, 535.
- [42] X.-S. Wang, H.-K. Kim, Y. Fujita, A. Sudo, H. Nishida, T. Endo, *Macromolecules* **2006**, *39*, 1046.
- [43] J. Araki, T. Kataoka, K. Ito, *Soft Matter* **2008**, *4*, 245.
- [44] C. Travelet, G. Schlatter, P. Hebraud, C. Brochon, A. Lapp, G. Hadziioannou, *Langmuir* **2009**, *25*, 8723.
- [45] A. Harada, J. Li, T. Nakamitsu, M. Kamachi, *J. Org. Chem.* **1993**, *58*, 7524.
- [46] J. Araki, K. Ito, *J. Polym. Sci., Part A: Polym. Chem.* **2005**, *44*, 532.
- [47] J. Araki, K. Ito, *J. Polym. Sci., Part A: Polym. Chem.* **2006**, *44*, 6312.
- [48] T. Ooya, N. Yui, *J. Controlled Release* **1999**, *58*, 251.
- [49] T. Ooya, M. Eguchi, N. Yui, *J. Am. Chem. Soc.* **2003**, *125*, 13016.
- [50] M. Tamura, A. Ueno, *Chem. Lett.* **1998**, *27*, 369.
- [51] M. Tamura, A. Ueno, *Bull. Chem. Soc. Jpn.* **2000**, *73*, 147.
- [52] J. Araki, K. Ito, *Polymer* **2007**, *48*, 7139.
- [53] S. Samitsu, J. Araki, T. Shimomura, K. Ito, *Macromolecules* **2008**, *41*, 5385.
- [54] C. Travelet, G. Schlatter, P. Hebraud, C. Brochon, A. Lapp, D. V. Anokhin, D. A. Ivanov, C. Gaillard, G. Hadziioannou, *Soft Matter* **2008**, *4*, 1855.
- [55] K. Mayumi, H. Endo, N. Osaka, H. Yokoyama, M. Nagao, M. Shibayama, K. Ito, *Macromolecules* **2009**, *42*, 6327.
- [56] C. Travelet, P. Hebraud, C. Perry, C. Brochon, G. Hadziioannou, A. Lapp, G. Schlatter, *Macromolecules* **2010**, *43*, 1915.
- [57] N. Jarroux, P. Guégan, H. Cheradame, L. Auvray, *J. Phys. Chem. B* **2005**, *109*, 23816.
- [58] T. Zhao, H. W. Beckham, *Macromolecules* **2003**, *36*, 9859.
- [59] R. Medrano, M. T. R. Laguna, E. Saiz, T. M. Pilar, *Phys. Chem. Chem. Phys.* **2003**, *5*, 151.
- [60] M. T. R. Laguna, J. Gallego, F. Mendicuti, E. Saiz, M. P. Tarazona, *Macromolecules* **2002**, *35*, 7782.
- [61] G. Marcelo, F. Mendicuti, E. Saiz, M. P. Tarazona, *Macromolecules* **2007**, *40*, 1311.
- [62] T. Kume, J. Araki, Y. Sakai, K. Mayumi, M. Kidowaki, H. Yokoyama, K. Ito, *J. Phys.: Conf. Ser.* **2009**, *184*.
- [63] D. V. O'Connor, W. R. Ware, J. C. Andre, *J. Phys. Chem.* **1979**, *83*, 1333.
- [64] J. R. Lakowicz, *Principles of Fluorescence Spectroscopy*, 3rd ed., Springer, New York **2006**, p. 97.
- [65] Tripos International, (2009), 1699 South Hanley Rd., St. Louis, Missouri 63144, USA.
- [66] M. Clark, R. D. Cramer III, O. N. Van, *J. Comput. Chem.* **1989**, *10*, 982.
- [67] M. J. Frisch, G. W. Trucks, H. B. Schlegel, G. E. Scuseria, M. A. Robb, J. R. Cheeseman, J. A. Montgomery, Jr., T. Vreven, K. N. Kudin, J. C. Burant, J. M. Millam, S. S. Iyengar, J. Tomasi, V. Barone, B. Mennucci, M. Cossi, G. Scalmani, N. Rega, G. A. Petersson, H. Nakatsuji, M. Hada, M. Ehara, K. Toyota, R. Fukuda, J. Hasegawa, M. Ishida, T. Nakajima, Y. Honda, O. Kitao, H. Nakai, M. Klene, X. Li, J. E. Knox, H. P. Hratchian, J. B. Cross, V. Bakken, C. Adamo, J. Jaramillo, R. Gomperts, R. E. Stratmann, O. Yazyev, A. J. Austin, R. Cammi, C. Pomelli, J. W. Ochterski, P. Y. Ayala, K. Morokuma, G. A. Voth, P. Salvador, J. J. Dannenberg, V. G. Zakrzewski, S. Dapprich, A. D. Daniels, M. C. Strain, O. Farkas, D. K. Malick, A. D. Rabuck, K. Raghavachari, J. B. Foresman, J. V. Ortiz, Q. Cui, A. G. Baboul, S. Clifford, J. Cioslowski, B. B. Stefanov, G. Liu, A. Liashenko, P. Piskorz, I. Komaromi, R. L. Martin, D. J. Fox, T. Keith, M. A. Al-Laham, C. Y. Peng, A. Nanayakkara, M. Challacombe, P. M. W. Gill, B. Johnson, W. Chen, M. W. Wong, C. Gonzalez, J. A. Pople, *MOPAC (AM1)*, included in the Gaussian 03 package, Gaussian 03, Revision C.02, edition, Gaussian, Inc., Wallingford, CT, USA **2004**.
- [68] J. Pozuelo, J. M. Madrid, F. Mendicuti, W. L. Mattice, *Comput. Theor. Polym. Sci.* **1996**, *6*, 125.
- [69] Y. Brunel, H. Faucher, D. Gagnaire, A. Rassat, *Tetrahedron* **1975**, *31*, 1075.
- [70] W. H. Press, S. A. Teukolsky, W. T. Vetterling, B. P. Flannery, *Numerical Recipes: The Art of Scientific Computing*, 3rd ed., Cambridge University Press, Cambridge **2007**.
- [71] C. Teucher, C. C. Michel, F. Hauser, D.-Y. Park, H. W. Beckham, G. Wenz, *Macromolecules* **2013**, *46*, 2.
- [72] W. Mormann, U. Michel, *Carbohydr. Polym.* **2002**, *50*, 201.
- [73] A. Harada, *Coord. Chem. Rev.* **1996**, *148*, 115.
- [74] K. I. Aly, *Polym. Int.* **1999**, *48*, 773.
- [75] J. Gironés, M. T. B. Pimenta, F. Vilaseca, C. A. J. F. de, P. Mutje, A. A. S. Curvelo, *Carbohydr. Polym.* **2007**, *68*, 537.
- [76] A.-A. M. A. Nada, S. Kamel, M. El-Sakhawy, *Polym. Degrad. Stab.* **2000**, *70*, 347.
- [77] J. Bravo, F. Mendicuti, E. Saiz, W. L. Mattice, *Macromol. Chem. Phys.* **1994**, *195*, 3411.
- [78] F. Mendicuti, W. L. Mattice, *Polym. Bull.* **1989**, *22*, 557.
- [79] I. B. Berlman, *Handbook of Fluorescence Spectra of Aromatic Molecules*, 2nd ed., Academic Press, New York **1973**.
- [80] J. Guillet, *Polymer Photophysics and Photochemistry: An Introduction to the Study of Photoprocesses in Macromolecules*, Cambridge University Press, London **1985**, p. 141.
- [81] A. Harada, M. Okada, J. Li, M. Kamachi, *Macromolecules* **1995**, *28*, 8406.
- [82] S. Loethen, T. Ooya, H. S. Choi, N. Yui, D. H. Thompson, *Bio-macromolecules* **2006**, *7*, 2501.